Korean J. Chem. Eng., 32(5), 826-836 (2015)
DOI: 10.1007/s11814-014-0246-5

pISSN: 0256-1115
eISSN: 1975-7220

Measurement of liquid film thickness in air - water two phase flows in conventional and mini channels using image processing

Arunkumar Seshadri, Swetha Mahadevan, and Venkatesan Muniyandi†

School of Mechanical Engineering, SASTRA University, Thanjavur, India
(*Received 23 February 2014 • accepted 24 August 2014*)

Abstract−The measurement and study of liquid films in the case of two phase flows is significant in many heat transfer and mass transfer applications, such as chemical process industries, micro reactors, coating processes and in boilers. The focus of the present study was to measure and characterize the thickness of the liquid films for various two phase flow regimes in conventional and in mini channels using a non-intrusive technique. Experiments were performed on tubes of diameters 0.6, 1.5, 2.6 and 3.4 mm. The superficial velocities of gas and liquid are in the range of 0.01-50 and 0.01-3 m/s, respectively. The flow patterns were recorded with a high speed camera. A method to determine the two phase flow velocity using image registration has been discussed. Morphological processing and gray scale analysis were used to determine the liquid film thickness and characterize the flow regimes. The flow patterns identified are bubbly, dispersed bubbly, slug, slug-annular, wavy-annular, stratified, and annular. The flow regimes were validated with flow maps available in the literature. The liquid film thickness was identified by distance transform technique in image processing. The magnitude of film thickness varied with liquid and gas flow velocities. The film thickness was represented in terms of capillary number. The variation in film thickness along the length of the flow regime has been discussed. A relation between the liquid film thicknesses measured using the non-intrusive image processing technique and capillary number for the conventional and mini tubes is proposed based on the analysis.

$$\frac{h}{d} = 2.03 Ca^{0.13} We^{0.52} \text{ for } Bo > 1$$

$$\frac{h}{d} = 1.08 Ca^{0.4} We^{0.35} \text{ for } Bo < 1$$

It is concluded from the proposed correlation that the variation in liquid film thickness is different for conventional and mini channels because of the effect of inertial dominance in conventional channels and viscous dominance in mini channels.

Keywords: Two Phase Flow, Flow Ppatterns, Liquid Film Thickness, Mini Channels

INTRODUCTION

Two phase flow is the simultaneous flow of two different substances or the same substance in two different phases. Two phase flow in horizontal channels has been investigated extensively because of its wide applications in nuclear science, chemical processing and refrigeration systems. The application of two phase flows in removing heat flux has been discussed by Howard et al. [1]. The characteristics of two phase flow are not completely understood because of its complexities. The study of mini channels is a prominent area of future research. This is attributed to the increased heat duties in the case of mini channels compared to conventional channels. This characteristic makes mini channel cooling technique play a significant role in nuclear fusion reactors and in optoelectronic devices.

Flow regime identification is important in identifying the characteristics of two phase flows such as heat transfer and pressure drop. Flow pattern recognition can be made by simple visual inspection of flow and more precisely with a high speed camera. Damianides and Westwater [2] used a high speed camera and presented flow maps for horizontal glass tubes of 1-5 mm diameter. The effect of tube diameter was further studied by Coleman and Garimella [3]. The transitions of various regimes and their dependence on hydraulic diameters and surface tensions were shown based on the experiments carried out. Kandlikar and Grande [4] classified the tubes based on diameters as Conventional channels, Mini channels, Micro-channels, Transitional channels and Transitional microchannels. Venkatesan et al. [5] studied two phase flow patterns in tubes of diameter 0.6, 1.2, 1.7, 2.6 and 3.4 mm using high speed camera. Unique flow patterns were observed based on tube diameters, and they concluded that the flow patterns formed were greatly influenced by the tube diameter.

Direct visualization of two phase flow becomes difficult with increase in two phase flow velocities. The analysis is still complicated for mini and micro channels. This necessitates new techniques for flow visualization. Harvel et al. [6] carried out real-time measurements in vertical annulus gas-liquid flow by X-ray tomography. The disadvantage of the techniques lies in the complexities involved in the process of detection of X-rays. Electrical sensors based on properties of differing dielectric constants commonly known as

†To whom correspondence should be addressed.
E-mail: mvenkat@mech.sastra.edu

capacitance probing technique have been efficient in determining the void fraction in case of liquid-gas flows and in liquid-liquid flows used in oil-water separation. Rzasa [7] has used a combination of capacitance and optical tomography for the identification of flow patterns in horizontal pipes. Ahmed and Ismail [8] used capacitance probing technique to measure void fraction for air-oil two phase flows. The advantage of capacitance probing method lies in accurate characterization of flows and measurement of void fraction in tubes. The difficulty lies in the determination of dielectric constants of the medium between the electrodes. Keska and Williams [9] did a review and compared the flow pattern detection techniques in air-water flows. Micro particle image velocimetry (PIV) is the predominant visual aspect for validating and analyzing different techniques in two phase flows since it can give other expedient information like the velocity flow field. Hasan [10] studied the PIV to formulate velocity measurements for two phase flows.

One of the vital parameters for which only few works are available in the literature is the distribution of liquid film layer along the walls of the tube. The study of liquid film is important in determining the heat transfer characteristics and the results of combustion processes. Liquid film formation is highly dependent on the forces acting on the fluids which in turn depend on the velocity of the fluid and the geometry of the tube. The presence of liquid film was initially reported by Fairbrother and Stubbs [11], who concluded that bubble velocity of bubble was faster than liquid slug because of the difference in the amount of liquid films present. After nearly three decades, Taylor [12] observed the liquid film thickness for flow with higher capillary number. A breakthrough in the field came when Bretherton [13] theoretically proposed the correlation for normalized liquid film thickness in terms of capillary numbers. Han and Shikazano [14] showed the role of inertial force on the thickness of liquid film in micro tubes.

The major difficulty associated in the study of liquid films is the measurement of film thickness in pipe of intricate sizes. The earliest methods were based on the measurement of conductivity. Dallman [15] used a very thin conductive probe to measure the film thickness. Chen et al. [16] used capacitance measurement technique to study the liquid film thickness based on the changes in void fraction. Schmitt et al. [17] used laser induced fluorescence to determine the properties of the liquid films. The use of Laser induced fluorescence is accurate, but care has to be taken to ensure a stable lighting effect. Moreover, there is a need to account for surface reflections. This necessitates a need to use a technique like image processing where there is no need for calibration.

Some of the recent advancements in imaging and image reconstruction [18-25] have also paved the path for the implementation of image processing techniques to study the two phase flows. Some of the earlier works on the application of image processing in two phase flows have dealt with determination of a particular type of flow regime. Mayor et al. [26] used a technique based on image analysis to study the gas-liquid slug flow along vertical pipes. Guo et al. [27] developed a wavelet analysis based edge detection techniques, which can be of vital potential in the application of multiphase flows.

The above literature shows that there is a need to develop a non-intrusive technique for the accurate determination of liquid film thickness in conventional and mini channels. Few works deal with the analysis of thickness of liquid films in top and bottom surface of the tube. Studying the variation in film thickness in the top and bottom surface of the tube helps in analyzing the inertial effect on the liquid film thickness. The present study focuses on applying image processing techniques for conventional and mini channels to measure liquid film thickness. As a preliminary analysis, a method for determining the flow patterns in tubes of four different diameters is done using Grayscale analysis and frequency density estimation techniques. The thickness of the liquid film is measured based on edge detection and mathematical morphology. The liquid film is analyzed for various values of superficial liquid and gaseous velocities. The liquid film thickness is studied based on the variation in non-dimensional parameters such as capillary number and Weber number. Based on scaling analysis, an empirical relation between the normalized liquid film thickness and capillary number is proposed for mini channels and conventional channels.

DESCRIPTION OF EXPERIMENTAL SETUP

The experimental setup is shown in Fig. 1. Water and air Rotameter are used to measure the volumetric flow rate of water and air from which superficial liquid and gaseous velocities are calculated. Normal tap water with TDS concentration 400 ppm is pumped using a 1400 LPH, 27 W water pump from an open tank. Air is blown at 1 bar by a 240 LPH, 3 W air pump. Air and water mixthoroughly in a T section. The T-section geometry used in the present case is the same used by Venkatesan et al. [5]. The test section is made of borosilicate smooth glass material. The experiment is carried out with four different tube diameters. 0.623 mm, 1.512 mm, 2.643 and 3.420 mm. The diameters were measured using the photographs taken and distance transformation technique explained in the next section. The wall contact angle of water was taken to be 0^{o}. The water was stored at 27-28 ^{o}C, and the flow rate was controlled by flow control valves. A developing length of 10 cm was provided between the test section and mixer section. The test loop was tested at periodic intervals for leaks. The important experimental parameters in two-phase flow study were the combination of superficial liquid and superficial gas velocities. In the present work, superficial velocities of gas and liquid are in the range 0.01-50 and

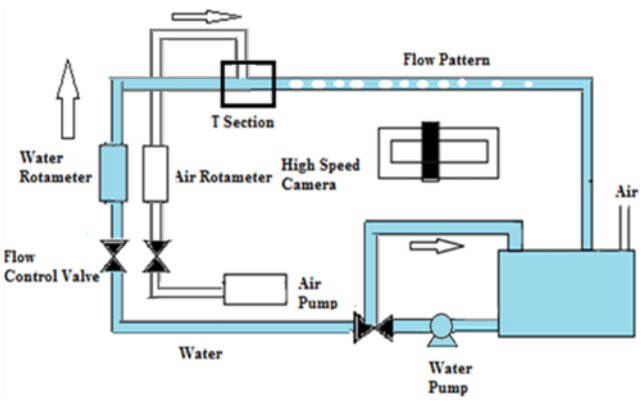

Fig. 1. Experimental setup.

0.01-3 m/s, respectively. Readings were taken after the steady state was reached for a particular superficial gaseous and liquid velocity.

The flow patterns were recorded with a high speed BASLER acA2000 Monochrome CMOS camera with a Navitar (Zoom 7000) lens. It can capture images at the rate of 1,500 fps for a 32×32 size resolution. The image was captured and subsequently analyzed frame by frame using Stream Pix Software. The image with pure liquid and air flow for the given tube diameter were also taken. Subsequently, the results were processed with suitable techniques and the pixel intensities were further analyzed to determine the pattern, film thickness and the pattern length.

1. Image Processing Techniques

1-1. Image Acquisition

The image was analyzed frame by frame in Stream pix software and the images were transferred in JPEG format. The image was read and analyzed in MATLAB using the image processing toolbox.

1-2. Image Filtering and Smoothing

The image captured was converted into a gray scale image for further processing. In the present analysis, the initial contrast adjustment was done using contrast-limited adaptive histogram equalization. The area of interest could be identified from the image after contrast enhancement. In the present work, linear filtering was used to remove the noise in which the value of an output pixel is a linear combination of the values of the pixels in the input pixel's neighborhood. The result of the filtering is the elimination of pixels in the image that have high deviation compared to the surroundings.

1-3. Morphological Operations, Image Binarization and Detection of Edges

In a morphological operation, the value of each pixel in the output image is in association with the corresponding pixel in the input image with its neighbors. Dilation adds pixels to the boundaries of objects in an image. On the contrary, erosion removes pixels from object boundaries. An opening transform denoted by I∘S implies dilation after erosion. The closing transform denoted by I•S, is defined as a dilation followed by an erosion. The top-hat filter is used to compute the morphological opening of the image and then subtracts the image from the original. The photographs obtained in these experiments have a dark background. Top hat transform was applied to these images to correct the background uniformity. A function was defined to perform the top-hat filter algorithm:

$$\tau = I - (I \circ S)$$

where τ represents the result of top-hat transform, I corresponds to the original image, S is the structuring element and "∘" is an operator indicating a opening transform, which means a erosion followed by dilation. Similarly, the bottom-hat filter was used to subtract the original image from its morphological closing.

When using both techniques together it is also possible to enrich the image contrast, thus helping in further operations. The Matlab function "imbothat" corresponds to the bottom-hat filter algorithm

$$\beta = I - (I \bullet S)$$

where β represents the result of bottom-hat transform, I corresponds to the original image, S is the structuring element and the operator "•" corresponds to a closing transform, which means a dilation followed by erosion.

The general edge detection operators like Canny, Sobel or Prewitt are difficult in detecting the edge clearly because of the curvature effects of the cylindrical shaped mini channel causing various interferences. So an effective application of combination of dilation and erosion is evaluated and one such technique gives an image that is later easily processed using the available operators. This technique is discussed in detail by Kritika et al. [28]. The high contrast image obtained after this process is converted to a binary image for further processes like edge detections. The method adopted by Kritika et al. [28] is used to effectively determine the edges.

1-4. Intensity Profile

The intensity profile of an image, otherwise called as Gray scale analysis, is used as a tool to classify the flow pattern. The set of intensity values along the line segment at points regularly placed is plotted with the increase in pixel distance. By properly selecting the line segment it is possible to visualize the differences in each type of flow.

1-5. Distance Transformation

Distance transform is a method to measure the separation of points in an image. Its algorithm is a simple combination of matrix algebra and the two-dimensional distance formula. The Quasi-Euclidean approach in distance transform measures the Euclidean distance along the vertical, horizontal and also diagonal lines. The diameter of the tube is measured by following the procedures in the earlier section. Knowing the diametrical distance the film thickness and the slug/Bubble length can be measured easily using this transform.

2. Measurement of Two phase Flow Regime Velocity

The two phase flow regime velocity is important in characterizing the film thickness measurement. Han and Shikazano [14] analyzed the thickness of liquid film in terms of capillary number, which in turn is dependent on two phase flow velocity. Hence, it is necessary to determine accurately the two phase flow regime velocity. In earlier literatures, videography was used generally for measuring the two phase slug velocity measurement. But for lengthy slug, this process becomes difficult. So the image registration technique used for two consecutive frames along with the distance formula provides a way for the slug velocity measurement. In the present case, a high speed camera was used for imaging at a constant speed and the time between two consecutive frames is a constant. For the case shown in Fig. 2 (two consecutive slugs in pink and green) the frame rate is 100 fps.

Fig. 2 shows the image after registering. The photographic length is measured to be 10 mm. So the distance passed by the slug in consecutive frame is given by 20/500 * 10 mm which is 0.4 mm. The velocity is 0.4 mm/(1/100) which is 0.04 m/s.

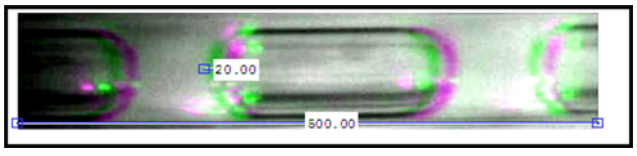

Fig. 2. Velocity determination for U_g=1.1 m/s, U_l=0.32 m/s in 3.4 mm tube.

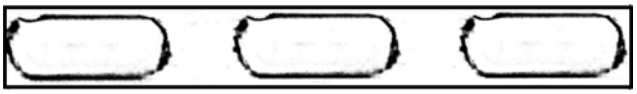

Fig. 3. Slug flow pattern observed U_g=1.1 m/s, U_l=0.32 m/s and the part of image obtained after processing in 3.4 mm tube.

RESULTS AND DISCUSSION

1. Preliminary Analysis: Flow Regime Identification

1-1. Slug Flow

A slug may be formed by the coalescence of smaller bubbles in conventional channels or compression of a bubble whose diameter is bigger than the diameter of the tube in mini/micro channels. Slug flow regime is characterized by a bullet shaped slug having a sharp nose at front and flat tail. Increasing the gaseous velocities leads to increase in slug length. Fig. 3 shows the image obtained after processing with the techniques discussed in an earlier section.

The pixel intensity levels in the processed image can be considered as a signal. By using the pixel intensity profile, the shape and size of the image can be well understood. The flow can be characterized as slug flow from the intensity profile. For the processed image the pixels of intensity around 255 indicates the liquid and that of irregular low intensities indicates the air slug. It is clear from the graph shown in Fig. 4 that the amount of pixels in high intensity values and low intensity values are nearly the slug flow, leading to a high void fraction which is a characteristic of slug flow. This can be made still clear from the frequency distribution graph shown in Fig. 5.

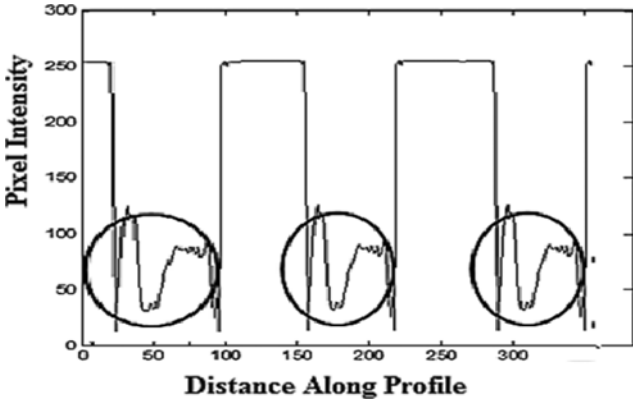

Fig. 4. Intensity profile along the center of the tube for a slug flow.

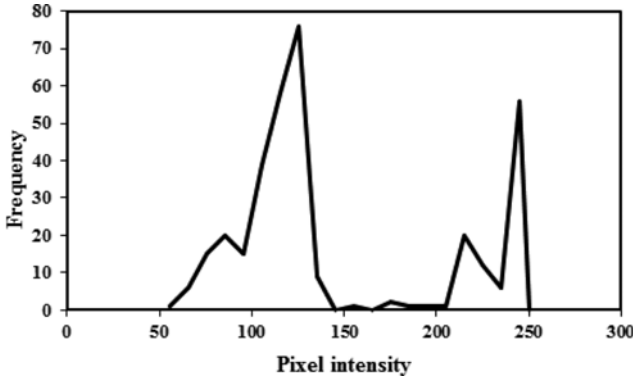

Fig. 5. Frequency distribution curve for slug flow.

Fig. 6. Slug train flow pattern observed U_g=1.8 m/s, U_l=0.52 m/s and the part of the image obtained after processing in 3.4 mm tube.

With the increase in u_g the slugs become close and a kind of flow pattern commonly known as slug train appears as shown in Fig. 6. An interesting observation is noted in the case of mini channels. At low gaseous velocities, a slug breaks away into smaller slugs and then into smaller bubbles. But at moderate velocities a long slug collapses into a bubble, a slug and then a tiny bubble again. This is similar to the observations of Daminades and Westwater [2].

1-2. Bubbly Flow

When the superficial velocity of the liquid is increased, the pattern observed is bubbly flow. The bubbly flow is categorized by spherical or non-spherical bubbles equal to or less than the channel diameter. The bubbles become spherical with the increase in superficial liquid velocity with moderate gaseous velocity. The processed image for bubbly flow is shown in Fig. 7.

The encircled regions are the area to be focused in Fig. 8. The lengthier zone of high value intensities around 255 compared to shorter one of intensities at lower values indicates a low void fraction clearly describing a bubbly flow. The frequency plot is shown in Fig. 9. The peak around 250 pixels indicates the majority of water,

Fig. 7. Bubbly flow observed U_g=0.3 m/s, U_l=0.9 m/s and the part of image obtained after processing in 2.6 mm tube.

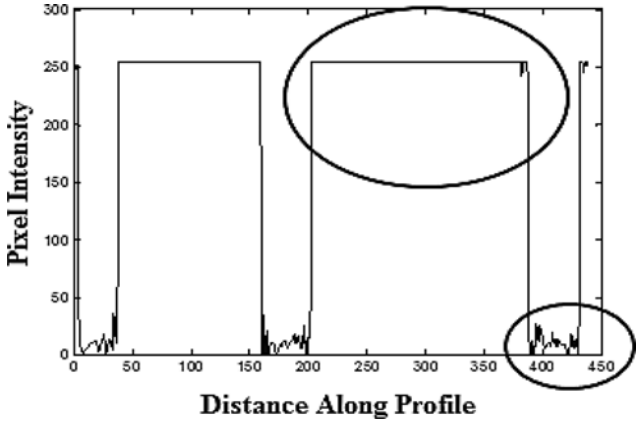

Fig. 8. Intensity profile along the center of the tube for a bubbly flow.

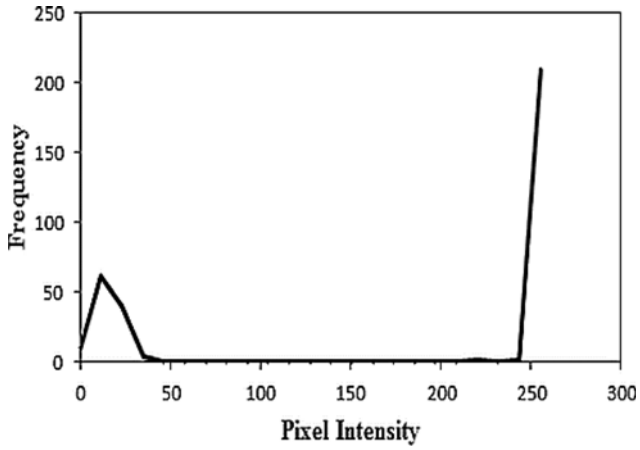

Fig. 9. Frequency distribution curve of bubbly flow.

Fig. 10. Bubble train U_g=1.95 m/s, U_l=1.1 m/s and the part of image obtained after processing in 3.4 mm tube.

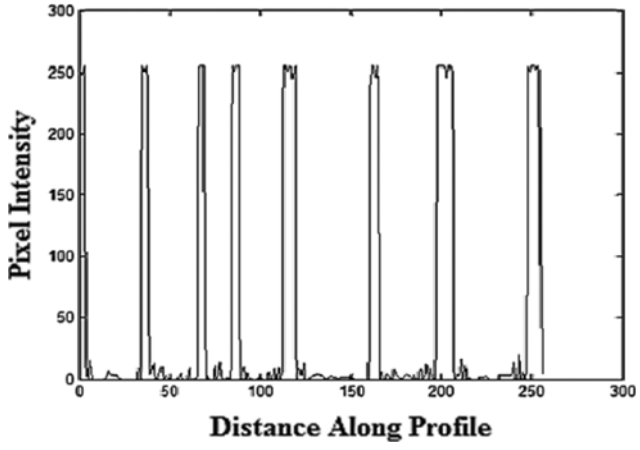

Fig. 11. Intensity profile along center of the tube for bubble train.

and a smaller peak at lower values indicates the presence of bubbles.

When there is a rise in superficial gaseous velocity there is an increase in amount of small sized bubbles flowing throughout as shown in Fig. 10. This flow pattern can be considered as a bubble train.

The continuous nature of the bubble is well indicated by the smaller peak in the intensity profile in Fig. 11.

1-3. Churn Flow

At very high gaseous velocities the bubbles occupy the top layer of the channel dispersed throughout the layer. This can be visualized from the processed image shown in Fig. 12. This flow is defined as the churn flow.

The intensity profile in Fig. 13 indicates a very high volume of water compared to air.

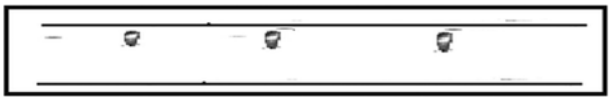

Fig. 12. Churn flow at U_g=2.29 m/s, U_l=1.22 m/s and the part of image obtained after processing in 3.4 mm tube.

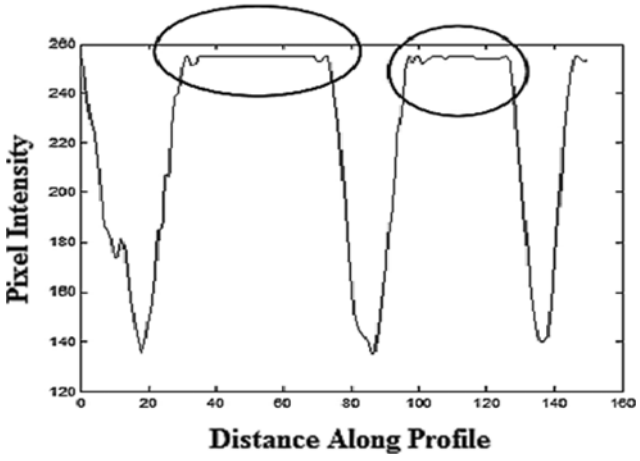

Fig. 13. Intensity profile at one-fourth of tube diameter from the top of the tube for churn flow.

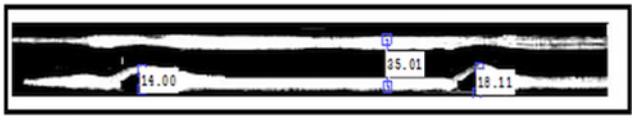

Fig. 14. Slug annular flow for U_g=7.85 m/s, U_l=0.52 m/s and the part of image obtained after processing in 1.5 mm tube.

1-4. Annular Flows

At low liquid velocities and very high gaseous velocities, slugs merge and the results in a type flow pattern called slug-annular flow as shown in Fig. 14.

The processed image shown in Fig. 14 is obtained by following the mathematical morphological operation described earlier followed by image thresholding. The threshold value was obtained in Matlab using the function imthresh(). Thresholding is based on the decision given as a conditioned input after receiving the threshold value to decide the pixel intensity above the threshold value to be closer to 255 and below the value to be closer to 0. Fig. 15 shows the analysis of the intensity profile along a line segment passing through the rise in liquid level.

Slugs with high velocities coalesce with each other and develop wavy appearance of the top surface of liquid, which is known as wavy annular. The photograph and the processed image are shown in Fig. 16(a) and the corresponding intensity profile is shown in Fig. 16(b).

The wavy annular can be clearly distinguished from the slug annular by considering the intensity profile along the line segment passing through the lower most surface of the liquid. At some portion there is a sudden fall in the intensity and it predominates over a period of time.

The other type of flow is observed for very high gaseous velocity

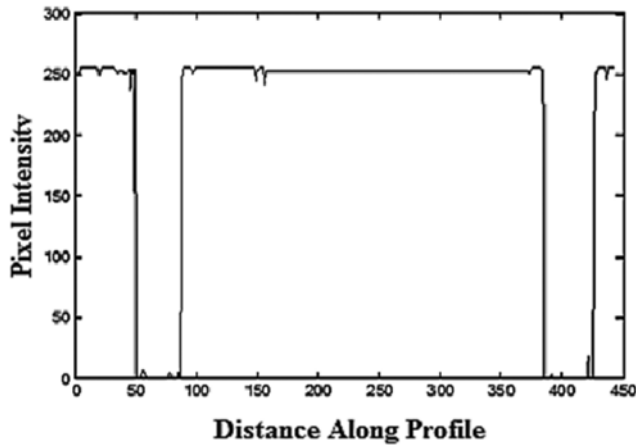

Fig. 15. Intensity profile for slug annular flows.

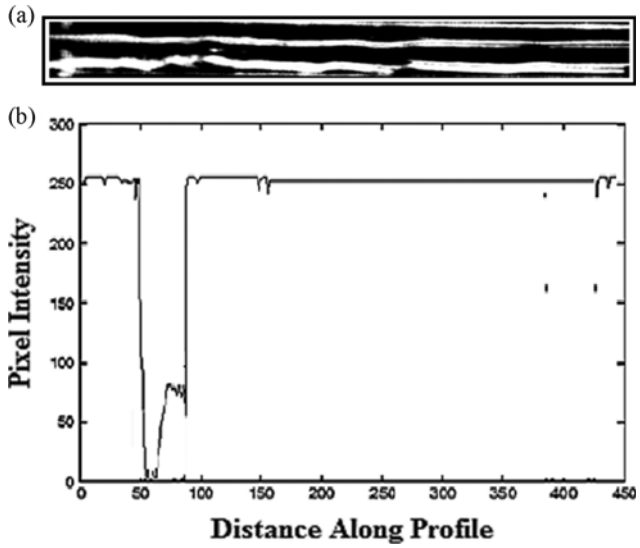

Fig. 16. (a) Wavy annular pattern for U_g=10.5 m/s and U_l=0.42 m/s and the part of image obtained after processing in 1.5 mm tube. (b) Intensity profile for annular wavy.

around 30 m/s. Fig. 17(a) illustrates the annular flow pattern observed for U_g=29.8 m/s and U_l=0.13 m/s. This is similar to annular wavy except for the absence of visible waves at the surface. The intensity profile along the lower most surface of the liquid is shown in Fig. 17(b).

1-5. Stratified Flows

Stratified smooth flow is defined as the pattern of flow in which the interface between the liquid and gas is a smooth straight line. The liquid and gas are completely separated. Since the amount of noise due to sudden changes in refractive indices is less in this case, the processed image can be obtained just by contrast enhancement using histogram stretching technique. Fig. 18 is the enhanced image portraying this type of flow.

It is clear from the figure that the dark regions are regions with water and the brighter one pertains to air. This can be seen from the intensity profile in Fig. 19.

Stratified smooth type of flow is similar to stratified smooth except

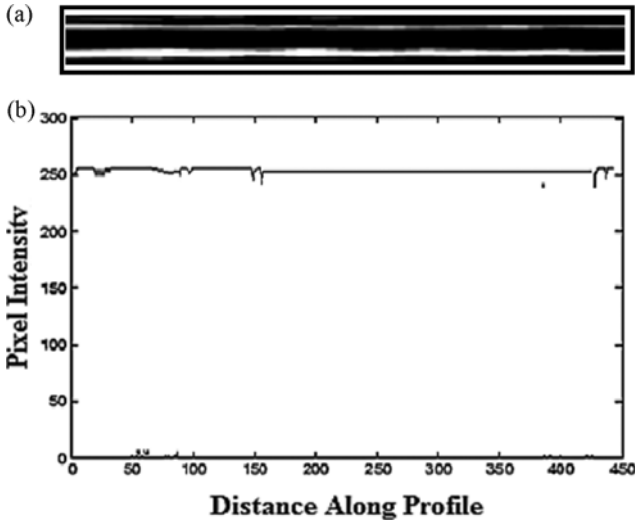

Fig. 17. (a) Annular flows for U_g=29.2 m/s and U_l=0.42 m/s and the part of image obtained after processing in 1.5 mm tube. (b) Intensity profile for annular flows.

Fig. 18. Stratified smooth flows U_g= 8.25 m/s, U_l=0.03 m/s and the part of image obtained after processing in 2.6 mm tube.

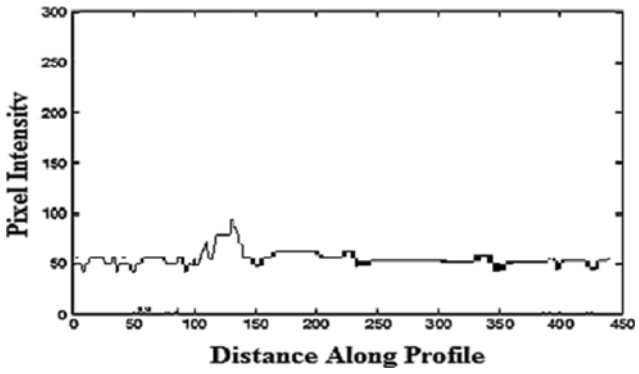

Fig. 19. Intensity profile for stratified smooth flows.

Fig. 20. Stratified wavy for U_g=7.85 m/s and U_l=0.04 m/s for and the part of image obtained after processing in 2.6 mm tube.

the appearance of waves at the air liquid interface. The stratified wavy pattern appears as shown in Fig. 20. It is the image obtained after contrast enhancement.

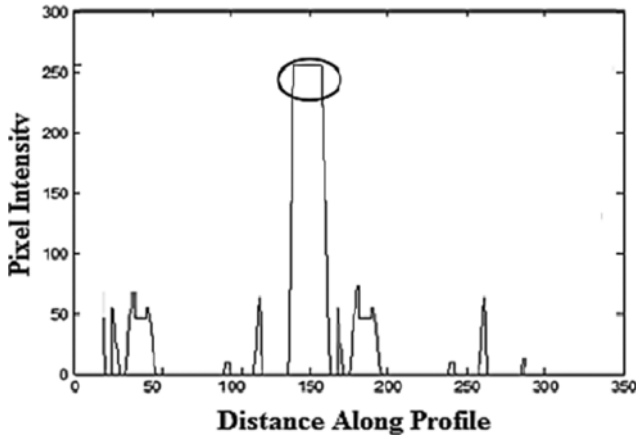

Fig. 21. Intensity profile for stratified wavy.

The intensity profile along a line segment passing through the midpoint is shown in Fig. 21. The length in the pixel intensity is high as the region of formation of wave.

1-6. Validation of the Results with Earlier Flow Maps

The results obtained after image processing and the classification of flows from the intensity plot are marked in a flow map. The results obtained are in good agreement with the results of Daminiades and Westwater [2] and Venkatesan et al. [5].

2. Measurement of Liquid Film Thickness

In the previous section, the identification of flow regime was dealt with to classify and characterize the flow patterns precisely. It can be clearly concluded from the processed image that it is possible to distinguish the liquid film and the air flow. Distance transform is used to calculate the film thickness based on the relative measurement of distances between the pixels. The formation of film is based on the nature of the viscous effects at the solid-liquid interface on the walls of the tube. However, the magnitude of the film thickness varies because of the effects of various forces like surface tension, inertial and body forces. The film thickness also varies across the flow regime at various intervals because of the presence of waves. In the present section, the various characteristics of liquid film thickness is studied.

2-1. Inertial and Non-inertial Dominance

The results of the image processing analysis for the four tube diameters are in Tables 1-4. Table 1 shows the value of minimum liquid film thickness at the top and bottom of the tube for a 3.4 mm diameter tube. From the values in Table 1 it can be inferred that the liquid film thickness at the bottom portion is much higher than at the top, because of higher density of water when compared with air. This indicates that the flow is gravity dominant. Table 2 gives the precise value of the liquid film thickness measured for different superficial liquid and gaseous velocities for 2.6 mm tube. Analyzing the film thickness for various flows and from Table 2 it is inferred that the variation in the liquid film thickness is nearly the same as observed in 3.4 mm tube. It is seen that there is a need for air at high flow rate to be injected to ensure a uniform liquid thickness, that is, the liquid film thickness at the bottom of the tube increases with increase in superficial liquid velocity. The gravitational force being predominant makes the water to settle at the bottom of the tube.

However, the case is opposite for superficial gaseous velocity. It is seen that the annular flow regimes occur at a higher superficial gaseous velocity. In other words, the thickness of the liquid film at the top surface increases with the increase in superficial gaseous velocities. But when it reaches a certain limit, there is no further

Table 1. Film thickness for various flows in 3.4 mm dia tube

S. no	Flow pattern image with distance transform	Flow characteristics	Average film thickness in top portion (mm)	Average film thickness in bottom portion (mm)
1.		Slug flow U_g=0.8 m/s U_l=0.6 m/s	0.8	1.21
2	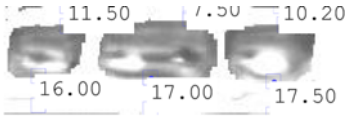	Slug train U_g=1.8 m/s U_l=0.52 m/s	0.93	1.417
3		Bubbly flow U_g=0.25 m/s U_l=0.92 m/s	0.495	0.7947
4		Bubble train U_g=0.25 m/s U_l=0.92 m/s	0.45	0.942
5	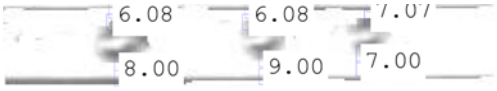	Churn flow U_g=0.25 m/s U_l=0.92 m/s	0.587	1.457

Table 2. Liquid film thickness in 2.6 mm tube

S. no	Flow pattern image with distance transform	Flow characteristics	Average film thickness in top portion (mm)	Average film thickness in bottom portion (mm)
1.		Bubbly flow U_g=0.32 m/s U_l=0.95 m/s	0.352	0.84
2	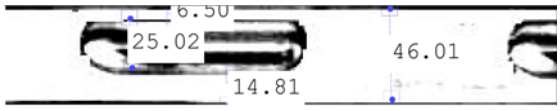	Slug flow U_g=1.1 m/s U_l=0.6601 m/s	0.36	0.7916
3	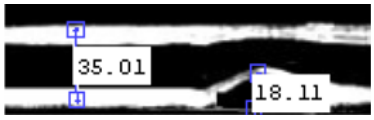	Slug annular U_g=7.85 m/s U_l=0.82 m/s	0.4136	1.07
4.	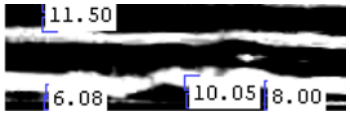	Wavy annular U_g=10.5 m/s U_l=0.42 m/s	0.67	0.93
5		Stratified flow U_g=8.25 m/s U_l=0.03 m/s		1.51

Table 3. Liquid film thickness for 1.5 mm tube

S. no	Flow pattern image with distance transform	Flow characteristics	Average film thickness in top portion (mm)	Average film thickness in bottom portion (mm)
1.	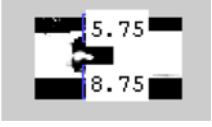	Bubbly flow U_g=2.6 m/s U_l=1.1 m/s	0.18	0.273
2	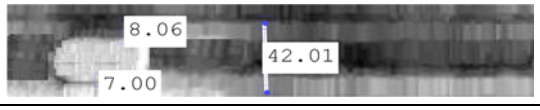	Slug flow U_g=1.8 m/s U_l=0.24 m/s	0.288	0.25
3	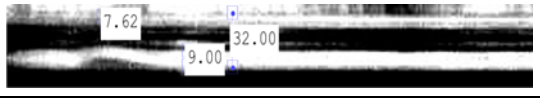	Slug annular U_g=10.4 m/s U_l=0.24 m/s	0.357	0.421
4	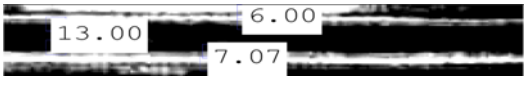	Annular flow U_g=29.08 m/s U_l=0.13 m/s	0.25	S. 0.47

increase in liquid film thickness in the top of the tube. Also, the thickness of the liquid film at the bottom of the tube decreases with increase in superficial gaseous velocity. Combining these two observations, it can be concluded that the gravitational force is responsible for limiting the increase in liquid film thickness at the top of the tube.

On the contrary, looking into Tables 3 and 4, the minimum liquid film thickness at the top and bottom of the tube is nearly the same. More interestingly, the thickness of the liquid film at the top of the tube in certain cases considered is higher than that at the bottom of the tube. This is in accord with earlier predictions that the surface tension force is predominant in tubes of diameter less than 2 mm (minichannels). So the flow regimes are non-inertial dominant. These regimes in these channels can be characterized as viscous or visco-inertial regime. The inertial effects can be considered or neglected by considering the variations in capillary number. This was discussed in detail by Eain et al. [29]. The dependence of liquid film thickness on capillary numbers is discussed in the forthcoming sections.

2-2. Variation in Liquid Film Thickness in Different Flow Regimes

It is seen from Table 1-4 that the liquid film thickness depends on the flow regime. For example, in a slug flow, the liquid film thick-

Table 4. Film thickness measurement in 0.6 mm tube

S. no	Flow pattern image with distance transform	Flow characteristics	Average film thickness in top portion (mm)	Average film thickness in bottom portion (mm)
1.		Bubbly flow U_g=3.93 m/s U_l=0.88 m/s	0.206	0.156
2	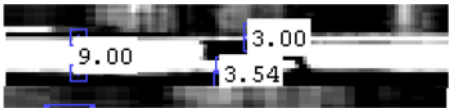	Slug flow U_g=1.96 m/s U_l=0.88 m/s	0.208	0.2348
3		Churn flow U_g=24.6 m/s U_l=1.38 m/s	0.284	0.145

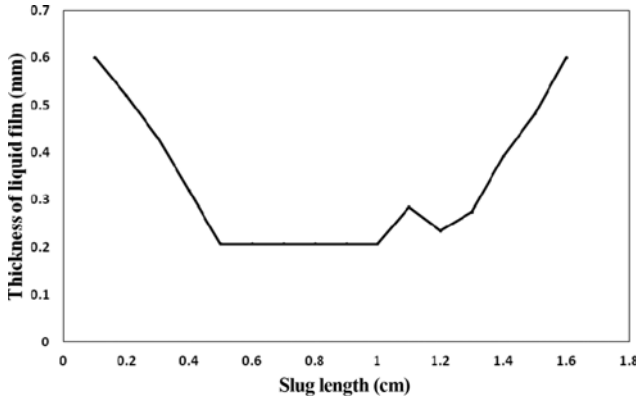

Fig. 22. Variation in liquid film thickness along the length of slug U_g=1.9 m/s, U_l=0.8 m/s in 0.6 mm tube.

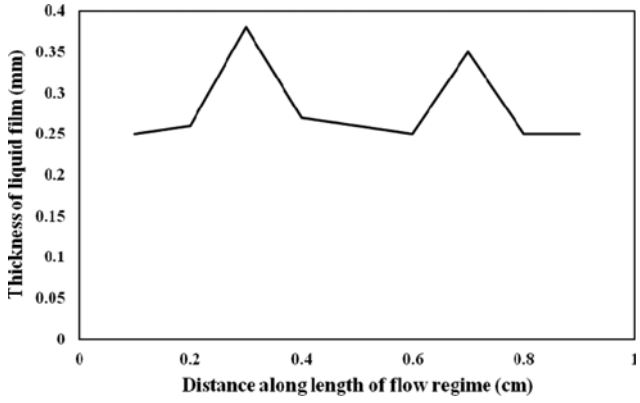

Fig. 23. Liquid film thickness variation along annular flows U_g= 29.18 m/s, U_l=0.18 m/s in 1.5 mm tube.

ness is at the maximum at the front and rear cap of the slug. The film thickness gradually decreases with increase in slug length. It reaches a constant magnitude after a particular slug length. The same trend is observed for slug of different lengths. A small wave appears at the rear end of the slug, which is shown as small peak at the right end of the graph shown in Fig. 22.

Bubbles show similar variations, but the case is slightly different

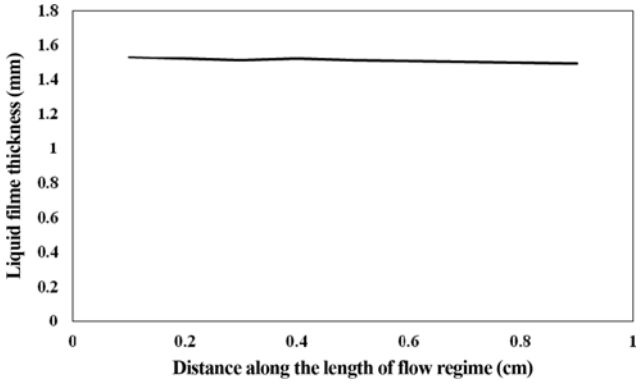

Fig. 24. Film thickness variation in stratified flows U_g=8.25 m/s U_l= 0.03 m/s and the part of image obtained after processing in 2.6 mm tube.

for dispersed bubbly or churn flow. The characteristic of a churn flow is the movement of fluid air dispersed in water on the top surface because of the effect of density of water. In this case, the liquid film thickness at the bottom surface is very high compared to that in top surface. This trend is observed even in the case of mini channels.

For annular flows, the thickness at the top and bottom depends on the nature of waves present at the surface of liquid film. The smaller peaks in the figure show the waves in the annular flows.

In stratified flows, air occupies the entire top surface and water stratifies at the bottom of the tube. So, liquid film thickness at bottom of the tube alone is considered. The liquid film is nearly constant for stratified flow as shown in Fig. 24.

2-3. Effect of Capillary Number of Liquid Film Thickness

It is clear from the analysis that the liquid film thickness depends on various factors like type of flow regime, superficial liquid and gaseous velocities and dimensions of the tube. So there is a need to characterize the liquid film thickness in terms of capillary numbers. In the present section, we attempted to obtain a correlation between the liquid film thickness and non-dimensional flow parameters for various flow regimes and tube diameters. Capillary number is defined as the ratio of viscous force to force due to surface tension and is represented as

$$Ca = \frac{\mu v}{\sigma}$$

Here μ is the dynamic viscosity of the liquid, v is the characteristic velocity and σ is the interfacial tension between the two surfaces. Weber number is the ratio of inertial force to the force due to surface tension:

$$We = \frac{\rho v^2 l}{\sigma}$$

where ρ is the density of the fluid and l is the characteristic length.

Bond number gives the relative influence of inertial force and surface tension force.

$$Bo = \frac{\rho g l^2}{\sigma}$$

The thickness is non-dimensionalized by dividing the magnitude of liquid film with the diameter of tube similar to the method followed by Han and Shikazona [14]. The variation in liquid film thickness with capillary number for conventional channels is given below.

$$\frac{h}{d} = 2.03 Ca^{0.13} We^{0.52} \text{ for } Bo > 1$$

Here h is the mean of minimum liquid film thickness at top and bottom surface of the tube and d is the diameter of the tube. The ratio of liquid film thickness and diameter of the tube is dependent on capillary number, Ca and Weber number, We. The mean deviation from the experimental data is found to be in the range 2.5-8.23%. It can be inferred that dependence of liquid film thickness on Weber number is high compared to capillary number. This indicates that the flow is inertially dominant.

The effect of capillary force is too little to dominate the flow, so it can be inferred that the flow is inertial dominated regime. When the same correlation is applied for flow in mini channels, the mean deviation from the experimental data is found to be 35.23-52%. It is clear that the correlation can be applied only for conventional channels. The variation in liquid film thickness with capillary number for mini channel is given below:

$$\frac{h}{d} = 1.08 Ca^{0.4} We^{0.35} \text{ for } Bo < 1$$

It can be clearly seen that for tube of diameter 0.6 mm, the liquid film thickness is more dependent on capillary force when compared with inertial force. It can be said that the flow has just entered visco-inertial regime. The mean deviation of the correlation from the experimental value is 0.3-4.32%. The above calculation is for cases in which the Bond number value is less than 1, indicating the dominance of surface tension force over the inertial force. This prediction of liquid film thickness based on Bond number is similar to pressure drop prediction by Venkatesan et al., [30] where the prediction of Chisholm's parameter was based on the Bond number.

Thus, we conclude that for conventional channels the effect of gravity is predominant on the liquid film thickness, butw the effect of viscosity is dominant in case of mini channels. This validates the reasoning of variation observed in the liquid film thickness in the top and bottom side of the tube in the case of mini channels and the conventional channels.

CONCLUSION

Two phase flow experiments were conducted on four different diameter tubes kept in horizontal position. A high speed camera was used to characterize the two phase flow pattern. Various image processing techniques were implemented to determine the liquid film thickness in two phase flows which are difficult to be determined by other methods. The distance transform was applied to the processed image to calculate the liquid film thickness. Analysis of liquid film thickness in various tubes clearly indicates the dominance of gravity (Bond number greater than 1) in the conventional tubes and surface tension effects in mini channel (Bond number less than 1). An empirical relation between liquid film thickness and non-dimensional flow parameters for the conventional and mini tubes is proposed based on the analysis. It is concluded that the liquid film thickness and its distribution in tube is dependent on the inertial and surface tension effects.

REFERENCES

1. J. A. Howard, P. A. Walsh and E. J. Walsh, *Int. J. Heat Mass Transfer*, **54**, 4752 (2011).
2. C. A. Damianides and J. W. Westwater, in *Proc. Second UK National Conf. on Heat Transfer*, Mechanical Engineering Publications, London (1988).
3. J. W. Coleman and S. Garimella, *Int. J. Heat Mass Transfer*, **42**, 2881 (1999).
4. S. G. Kandlikar and W. J. Grande, *Heat Transfer Eng.*, **24**, 3 (2003).
5. M. Venkatesan, S. K. Das and A. R. Balakrishnan, *Can. J. Chem. Eng.*, **35**, 531 (2010).
6. G. D. Harvel, K. Hori, K. Kawanishi and J. S. Chang, *Nucl. Instrum. Methods Phys. Res. A*, **371**, 544 (1996).
7. M. R. Rzasa, *Metrology Meas. Systems XIV*, **2**, 291 (2007).
8. W. H. Ahmed and B. I. Ismail, *Recent Patents Elect. Eng.*, **1**, 1 (2008).
9. J. K. Keska and B. E. Williams, *Exp. Thermal Fluid Sci.*, **19**, 1 (1999).
10. Y. A. Hassan, T. K. Blanchat, C. H. Seeley and R. E. Canaan, *Int. J. Multiphase Flow*, **18**, 371 (1992).
11. F. Fairbrother and A. E. Stubbs, *J. Chem. Soc.*, **6**, 527 (1935).
12. G. Taylor, *J. Fluid Mech.*, **10**, 161 (1961).
13. F. P. Bretherton, *J. Fluid Mech.*, **10**, 166 (1961).
14. Y. Han and N. Shikazono, *Int. J. Heat Fluid Flow*, **31**, 631 (2010).
15. J. C. Dallman, PhD Thesis, University of Illinois at Urbana-Champaign, Urbana, IL (1978).
16. X. Chen, T. Butler and J. P. Brill, *Proceedings of the ASME Heat Transfer Division at the International Mechanical Engineering Congress and Exposition*, **336**, 201 (1996).
17. R. L. Schmitt, W. H. Stevenson and H. C. Stevenson, *Proceedings of the Inspections, International Congress of Applications of Measurement and Control Symposium, Lasers and Electro-Optics*, 33 (1982).
18. P. R Muduli and U. C. Pati, In *Intelligent Computing, Networking, and Informatics*, **1**, 359 (2014).
19. N. Dietrich., K. Loubiere, M. Jimenez, G. Hebrard and C. Gourdon, *Chem. Eng. Sci.*, **1**, 100 (2013).

20. C. Mauger, L. Mees, M. Michard and M. Lance, *Int. J. Multiphase Flow*, **58**, 301 (2014).
21. R. Banerjee and S. G. Kandlikar, *J. Power Sources*, **247**, 9 (2014).
22. S. U. Jung, H. W. Park and S. J. Lee, *J. Synchrotron Radiation*, **21**, 1160 (2014).
23. J. Y. Liang, *Appl. Mech. Mater.*, **511**, 550 (2014).
24. Y. Yamada, *IEEE Conference on Asia-Pacific Synthetic Aperture Radar* (2013).
25. K. Singh and R. Kapoor, *Pattern Recognition Letters*, **36**, 10 (2014).
26. T. Mayor, A. Pinto and J. Campos, *Chem. Eng. Sci.*, **63**, 3614 (2008).
27. F. Guo, Y. Yang, B. Chen and L. Guo, *Powder Technol.*, **1**, 202 (2010).
28. I. Kritika, S. Shridharani, S. Arunkumar and M. Venkatesan, In *IEEE International Conference on Computational Intelligence and Computing Research (ICCIC)* (2013), DOI:10.1109/ICCIC.2013.6724169.
29. M. G. Eain, V. Egan and J. Punch, *Int. J. Heat Fluid Flow*, **44**, 515 (2013).
30. M. Venkatesan, S. K. Das and A. R. Balakrishnan, *Exp. Therm. Fluid Sci.*, **35**, 531 (2011).